ChemComm

COMMUNICATION

View Article Online
View Journal | View Issue

Cite this: *Chem. Commun.*, 2021, **57**, 1478

Received 17th October 2020,
Accepted 22nd December 2020

DOI: 10.1039/d0cc06922a

rsc.li/chemcomm

Spontaneous anion-exchange synthesis of optically active mixed-valence $Cs_2Au_2I_6$ perovskites from layered $CsAuCl_4$ perovskites†

Bhawna, [a] Mrinmoy Roy, [a] Vikram, [a] Hitesh Borkar, [ab] Aftab Alam [a] and M. Aslam*[a]

$Cs_2Au_2I_6$, a lead-free photovoltaic material, has been synthesized *via* controlled and systematic addition of hydroiodic acid (HI) to $CsAuCl_4$. X-ray diffraction studies suggest the formation of $Cs_2Au_2I_6$ when a threshold concentration of HI is added to $CsAuCl_4$. The final compound shows good stability against light, oxygen and moisture and at temperatures up to 140 °C without any phase degradation. The stability of $Cs_2Au_2I_6$ is also confirmed by its high negative formation energy and the convex hull diagram constructed using Density Functional Theory (DFT). Absorption studies suggest an abrupt band shift from 2.31 eV to 1.06 eV when HI concentration reaches the threshold limit (~100 μl). A sharp absorption edge was found for $Cs_2Au_2I_6$ with an Urbach energy of 59 meV, indicating lower structural disorder and higher crystallinity.

Organic–inorganic (hybrid) as well as inorganic lead halide perovskites, ABX_3 (A = Cs^+, methylammonium, MA^+, formamidinium, FA^+; B = Pb^{2+}; X = Cl^-, Br^-, I^-), have turned out to be a promising class of photovoltaic absorber. In a short time, their photoconversion efficiency (PCE) has jumped to 25.1%,[1] from a scanty value of 3.8%.[2] At present, the main challenges on device research front are the toxic nature of lead (Pb) and their long-term stability.[3] Double perovskites are very promising alternatives to lead perovskites, which offer the required stability with less toxicity.[4–6] However, to date, only a PCE of 1–3% has been achieved in these compounds.[7–9] This poor PCE performance is either due to a large or an indirect bandgap present in these systems.[10,11] A non-toxic and stable perovskite with a direct bandgap of 1.2–1.6 eV (overlapping the visible solar range) is still an urgent need in the era of hybrid-halide photovoltaics.

$Cs_2Au_2I_6$ is a fascinating jet black colour old material discovered in 1922 by H.L. Wells.[12] These halides attracted the attention of researchers again in the 1980s as materials for superconductors.[13] The crystal structure of $A_2Au_2X_6$ (A = Cs, X = Cl, Br, I) appears as a distorted 3D-framework due to the charge disproportion of Au in +1 and +3 oxidation states.[14] In 1994, N. Kojima *et al.* for the first time reported the Jahn–Teller distortion driven by the $Au^{1+}/Au^{3+} \rightarrow Au^{2+}$ transition.[15] Kojima further reported the semiconductor-to-metal transition in $Cs_2Au_2I_6$ at room temperature (but higher pressure) due to the dynamic two-electron exchange between Au^{1+} and Au^{3+}, signifying highly mobile bipolarons.[16] Now, after a gap of three decades, in a recent theoretical simulation by Debbichi *et al.* $Cs_2Au_2I_6$ has been proposed as a very promising photovoltaic absorber due to an optimal band gap of 1.21 eV, arising from the charge disproportionation (Au^{1+}/Au^{3+}) present in the system. This also makes the quaternary structure inherit all properties like a double perovskite.[17] However, there are no experimental perspectives on the optical properties of $Cs_2Au_2I_6$ from the solar cell application viewpoint.

Here, we fabricate the $Cs_2Au_2I_6$ compound systematically and investigate its optical properties experimentally in the light of photovoltaic utility and suitability. First, we demonstrate experimentally that $CsAuCl_4$ can be formed easily at low temperatures of 5–10 °C using the precipitation approach. Surprisingly, the controlled addition of iodide in the form of HI (55% aqueous) then renders the $Cs_2Au_2I_6$ phase. Theoretical calculations also suggest that the $CsAuI_4$ phase is inherently unstable. Using absorption spectroscopy, we find the optical band gap of $CsAuCl_4$ to be 2.31 eV; however, at a critical amount of iodide, it suddenly lowers to 1.1 eV. Additionally, these gold halides are quite stable toward heat (up to 140 °C) as well as a humidity of 65% under ambient conditions. The main benefit is not only the non-toxic nature of Au but also the direct nature of bandgap as compared to double perovskites.

A simple precipitation technique was employed to obtain $CsAuCl_4$ and HI treated counterparts (see ESI† for details).

[a] *Department of Physics, Indian Institute of Technology Bombay, Mumbai 400076, India. E-mail: m.aslam@iitb.ac.in*
[b] *Department of Physics, National Institute of Technology, Warangal, Telangana 506004, India*

† Electronic supplementary information (ESI) available: Synthesis and characterisation, and computational details. See DOI: 10.1039/d0cc06922a

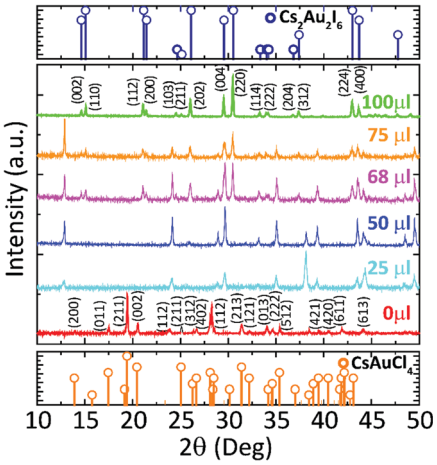

Fig. 1 XRD patterns of the $CsAuCl_4$ compound (x = 0 µl) and HI (x = 25, 50, 68, 75 and 100 µl) treated compounds. Compounds with x = 0 and x = 100 match with the JCPDS data of $CsAuCl_4$ (orange) and $Cs_2Au_2I_6$ (blue), respectively.

Powder X-ray diffraction (XRD) studies were performed to track the evolution of the $Cs_2Au_2I_6$ structure with subsequent addition of HI into the $CsAuCl_4$ solution (Fig. S1, ESI†). Fig. 1 presents the XRD profiles, which indicate that phase pure $CsAuCl_4$ is formed at moderately low temperatures of 5–10 °C when HI is not added into the solution. Rietveld refinement reveals that all the observed peaks can be indexed to the monoclinic space group $C2/c$ with lattice parameters: a = 14.07 Å, b = 6.25 Å, c = 9.59 Å, α = 90°, β = 115° and γ = 90° (Fig. S2, ESI†). Furthermore, the as-formed precipitate ($CsAuCl_4$) was used without any separation or filtration and was dissolved fully by adding 5 ml of DI water. The XRD profile of the compound (with 25 µl of HI addition) shows peaks corresponding to Au metal and AuI (Fig. S3(a), ESI†). As the concentration of HI is increased to 50 µl, the prominent AuI phase (JCPDS 015-0521) is formed. Furthermore, when the HI concentration is increased to 68 µl, the peaks corresponding to $Cs_2Au_2I_6$ are prominent with subdued impurity peaks of AuI (Fig. S3(b), ESI†). The phase pure $Cs_2Au_2I_6$ compound (without any trace of impurities) was obtained at a threshold of 100 µl of HI. The XRD pattern of $Cs_2Au_2I_6$ shows split peaks at 14.64° and 15.15° corresponding to (002) and (110) planes and also at 21.11° and 21.46° corresponding to (112) and (200) planes. Such a feature gives a clear indication that $Cs_2Au_2I_6$ crystallizes in the tetragonal phase and from Rietveld refinement, it is shown that it belongs to the space group $I4/mmm$ with lattice parameters: a = 8.28 Å, b = 8.28 Å, c = 12.08 Å and $\alpha = \beta = \gamma$ = 90° (Fig. S4, ESI†). The increase in the concentration of HI beyond the threshold value of 100 µl renders phase pure $Cs_2Au_2I_6$ without any trace of impurity peaks in the XRD data (Fig. S5, ESI†).

The stoichiometry of $CsAuCl_4$ and $Cs_2Au_2I_6$ was then confirmed by energy dispersive X-ray spectroscopy (EDS), which shows that the atomic ratios of Cs/Au and Cl/Au are 1.14 and 3.99 for $CsAuCl_4$, whereas the atomic ratios of Cs/Au and I/Au come out to be 0.9 and 2.8 for $Cs_2Au_2I_6$, respectively, which is consistent with the crystallographic compositions

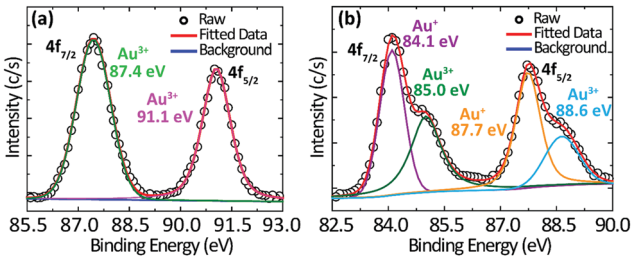

Fig. 2 (a) $CsAuCl_4$ reveals a signal from the 4f Au^{3+} state only, whereas (b) $Cs_2Au_2I_6$ shows signals from both Au^{1+} and Au^{3+} states as a result of spin–orbit splitting.

(Fig. S6, ESI†). Interestingly, the compound stabilizes in the $CsAuCl_4$ phase in the case of only Cl precursors, while the addition of iodine (as HI) renders the $Cs_2Au_2I_6$ phase (not $CsAuI_4$). Only the formation of $CsAuCl_4$ has been reported in the literature,[18] while there is no observation of the $Cs_2Au_2I_6$ phase under systematic iodide addition so far.

X-ray photoelectron spectroscopy (XPS) measurements were performed to investigate the electronic state of Au in $CsAuCl_4$ and $Cs_2Au_2I_6$ compounds (Fig. S7, ESI†). The high-resolution photoelectron spectrum [Fig. 2(a)] shows two peaks, Au $4f_{7/2}$ (87.4 eV) and Au $4f_{5/2}$ (91.1 eV), separated by a difference of 3.7 eV as a result of the spin–orbit splitting of Au^{3+} state only.[19] On the contrary, a reasonably broad doublet with two distinct humps in $Cs_2Au_2I_6$ indicates the presence of two different species of gold. Here, the Au $4f_{7/2}$ peak is deconvoluted into two sub-peaks with binding energies of 84.1 eV (Au^{1+}) and 85.0 eV (Au^{3+}). Similarly, the Au $4f_{5/2}$ peak is further deconvoluted into two sub-peaks at binding energies of 87.7 eV (Au^{1+}) and 88.6 eV (Au^{3+}) [Fig. 2(b)].[19] The contributions from Au^{1+} and Au^{3+} are separated by a small difference (0.9 eV) in binding energy due to the presence of very strong charge-transfer interactions between the bridged iodine networks of –I–Au^{1+}–I–Au^{3+}–.[20] Due to the presence of two kinds of valence states, linear $[Au^{1+}I_2]^-$ and square planar $[Au^{3+}I_4]^-$ networks with halogen surroundings are formed. These two networks sit together to form a 3D distorted corner-sharing octahedral framework of –I–Au^{1+}–I–Au^{3+}, which is no different than a 3D perovskite structure as can also be seen in Fig. S8, ESI.†

Fig. 3(a) shows the diffuse reflectance (DR) spectra of the sample with the addition of x = 0, 25, 50, 68, 75 and 100 µl of HI into the aqueous solution of $CsAuCl_4$. The pseudo-absorption

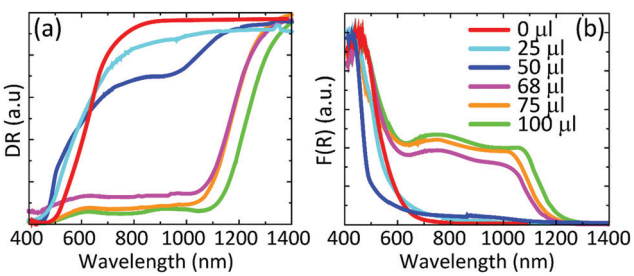

Fig. 3 (a) Variance of DR spectra of $CsAuCl_4$ with gradual addition of HI and (b) pseudo-absorption data extracted using the K–M equation.

data shown in Fig. 3(b) were then extracted from the reflectance data using the Kubelka–Munk (K–M) equation (details in ESI†). The pseudo-absorption spectrum of the $x = 0$ μl sample exhibits a sharp absorption edge at around 600 nm. The spectrum changes with an onset [for $x = 68$ μl sample, Fig. 3(b)] appearing near the visible range, indicating the appearance of the $Cs_2Au_2I_6$ phase, which gets matured in the green curve (x = 100 μl) illustrating that the $Cs_2Au_2I_6$ pure phase has emerged (confirmed by the XRD studies also) with a complete swamp and absorption onset at 1150 nm. The sharp absorption onset of $Cs_2Au_2I_6$ is associated with a high absorption coefficient of 7.01×10^4 cm^{-1} at 1.4 eV (near the bandgap value). This value is of the same order of magnitude as that of $MAPbI_3$ within the visible light range, suggesting strong optical absorption.[21] The absorption spectrum consists of a sharp shoulder followed by a band-to-band transition and the exponential tail. The slope of this tail (Urbach energy) represents a disorder in the system, wherein trap states are formed due to the variation of the position of the band edges spatially or temporally.[22] The low value of Urbach energy obtained for $Cs_2Au_2I_6$ (59 meV) (Fig. S9, ESI†) illustrates the lower degree of structural defects and hence, good crystallinity in the $Cs_2Au_2I_6$ phase. The value of Urbach energy obtained for $Cs_2Au_2I_6$ is only slightly larger than those of the hybrid lead triiodide perovskite ($MAPbI_3$ ~15 meV) and copper indium gallium selenide (CIGS ~25 meV), which indicates the well-ordered microstructure that is essential for the high-performance photovoltaic activity observed in perovskites.[23]

In order to find the optical band gap, a graph (Tauc plot) of $[F(R)hv]^{1/\gamma}$ *vs.* hv was plotted, wherein $\gamma = 1/2$ and 2 for direct and indirect transitions, respectively. The bandgap varies from 2.31 eV to 1.06 eV when x (HI concentration) changes from 0 to 100 μl [Fig. 4(a)–(f)]. Using the Tauc plot, the direct bandgap in $Cs_2Au_2I_6$ [Fig. 4(f)] is found to be 1.06 (±0.05) eV.

Ab initio DFT calculations were performed to assess the chemical stability of $CsAuCl_4$, $CsAuI_4$ and $Cs_2Au_2I_6$ (Table S1, ESI†) by simulating their formation energies (ΔE_f). We have also presented ΔE_f of $MAPbI_3$ for the sake of comparison. The decomposition pathways for each of these compounds are shown in the Computational details Section of the ESI.† The high negative value of ΔE_f for $CsAuCl_4$ indicates that its formation is thermodynamically impulsive and stable. The addition of HI to $CsAuCl_4$, however, yields a positive formation energy for $CsAuI_4$, suggesting it to be in an unstable phase. Fig. 5(a) shows a 2D formation energy contour plot for all the stable binary and ternary compounds with respect to Cs, Au and I. Evidently, $Cs_2Au_2I_6$ is highly stable with ΔE_f of -733.02 meV $atom^{-1}$. In order to assert the stability of $Cs_2Au_2I_6$ *via* the decomposition pathway given by eqn (3) in the ESI,† a 3D convex hull was simulated with respect to the reactants (AuI, AuI_3 and CsI), as shown in Fig. 5(b). It is evident from Fig. 5(b) that $Cs_2Au_2I_6$ lies below the plane containing the reactants, which signifies the feasibility of the proposed reaction pathway. These preliminary calculations fully support our experimental findings which confirm that the formation of $Cs_2Au_2I_6$ after the treatment of $CsAuCl_4$ with HI is more favourable than the formation of $CsAuI_4$. It should also be noted that the simulated formation enthalpy of $MAPbI_3$[24] in the tetragonal phase is less negative than that of $Cs_2Au_2I_6$, hinting towards a comparatively higher stability of the latter.

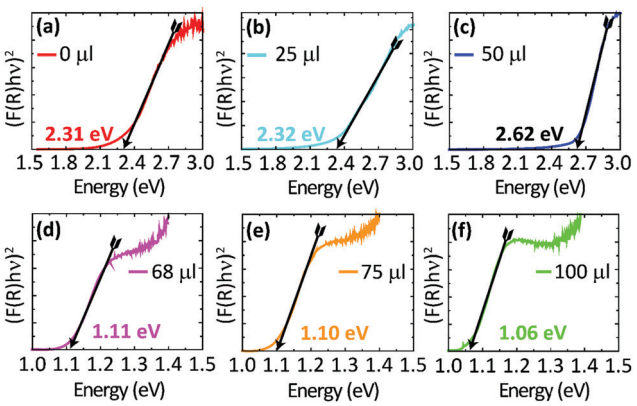

Fig. 4 (a–f) Tauc plots for various HI substituted samples to extract the direct bandgap using a graph of $[F(R)hv]^2$ *vs.* hv.

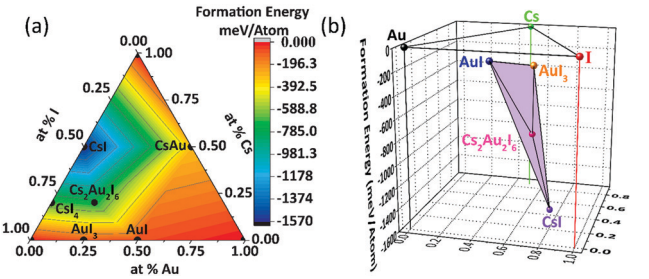

Fig. 5 (a) The 2D formation energy contour plot showing all the possible stable binary and ternary compounds with respect to the constituent elements (Cs, Au and I). Various colors represent the scale of formation energy values, as per the color bar adjacent to the plot; (b) the 3D convex hull diagram showing the stability of $Cs_2Au_2I_6$ with respect to the reactants (AuI, AuI_3 and CsI).

After addressing the toxicity concerns, with gold appearing to be a good choice in place of lead and confirming the optimal direct bandgap of ~1.1 eV, we further evaluated the stability of $Cs_2Au_2I_6$ against oxygen/moisture and heat degradation. The $Cs_2Au_2I_6$ sample was exposed to light under ambient conditions (humidity: 40–65% ± 5%). The visual inspection of the sample showed no sign of color change (it remained jet black). The XRD analysis of the sample was performed at regular time intervals [Fig. 6(a)], which confirmed no deterioration in the phase of $Cs_2Au_2I_6$ for nearly one and a half months. The results of a systematic ageing study of $Cs_2Au_2I_6$ for a longer period are shown in Fig. S10, ESI.† In contrast, $MAPbI_3$ hydrolyzes to PbI_2 within a week making it unfit for outdoor applications.[24] These observations confirm that the proposed material $Cs_2Au_2I_6$ could be a promising material for developing stable lead-free perovskite solar cells.

Next, $Cs_2Au_2I_6$ powder was tested for its stability toward heat (under vacuum conditions though) with temperature ranging from RT to 200 °C. As shown in Fig. 6(b), the phase remains

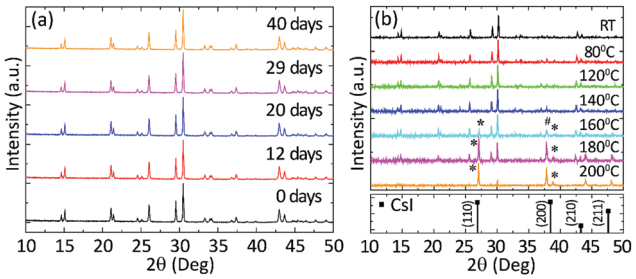

Fig. 6 (a) XRD patterns of $Cs_2Au_2I_6$ showing stability under ambient conditions with no deterioration in phase. (b) Temperature dependent XRD patterns of $Cs_2Au_2I_6$ recorded in the temperature range from RT to 200 °C. The * and # signs represent the peaks corresponding to the side phase of CsI and Au, respectively.

intact until 140 °C, and with a further increase in temperature, a peak starts to appear at $2\theta = 27.13^\circ$ which corresponds to CsI (JCPDS No.: 04-0528). This peak keeps on increasing in intensity, while the most prominent peak at $2\theta = 30.22^\circ$ corresponding to the (220) plane of the $Cs_2Au_2I_6$ phase decreases continuously. This degradation is mainly due to the fact that gold chloride starts decomposing at a temperature of 160 °C and above.[25]

In comparison to $Cs_2Au_2I_6$ reported herein, the hybrid gold-based counterpart (namely $MA_2Au_2(I/Br)_6$,) was found to be optically similar, however, degrades very quickly within a few days in the presence of moisture.[26] Also, there are layered gold perovskites ($MA_2Au_2(Cl/Br)_6.H_2O$) which show a quite large band-gap ($\sim$2.5 eV), beyond the ideal visible range,[27] as compared to $Cs_2Au_2I_6$. Unlike other recent reports on hybrid gold-based halide perovskites, where the structure and the optical gap sensitively depend on the cationic size,[28] $Cs_2Au_2I_6$ is structurally simpler, more robust and shows quite favourable optical properties which are ideal for future opto-electronic devices.

In conclusion, we have experimentally demonstrated the formation of $CsAuCl_4$ using the precipitation method which renders the $Cs_2Au_2I_6$ phase *via* controlled addition of HI. The inherent instability of $CsAuI_4$ leads to the emergence of highly stable $Cs_2Au_2I_6$, as also confirmed by the convex hull diagram simulated using *ab initio* DFT calculations. Absorption studies revealed the bandgap of $CsAuCl_4$ to be 2.31 eV. However, at a critical concentration of HI, it conforms to $Cs_2Au_2I_6$, with an optical bandgap of $\sim$1.1 eV, making it a promising visible-light absorber. Also, $Cs_2Au_2I_6$ remains stable under ambient conditions and is resistant to temperatures up to 140 °C. Our results suggest that mixed-valence gold halide perovskites are potential alternatives to lead hybrid perovskites and will be utilized in photovoltaics in the near future.

M. A. and Bhawna conceptualized the problem. The experiments were performed by Bhawna. M. R. and H. B. helped in analyzing the data. A. A. and Vikram conceived the theoretical ideas and Vikram performed the DFT calculations. M. A. and A. A. approved the final version of the manuscript.

This project was supported by NCPRE, IIT Bombay. The authors would like to thank SAIF, IRCC and IIT Bombay Nanofabrication facility for providing access to the characterization facilities.

Conflicts of interest

There are no conflicts to declare.

References

1 G. Nogay, F. Sahli, J. Werner, R. Monnard, M. Boccard, M. Despeisse, F. J. Haug, Q. Jeangros, A. Ingenito and C. Ballif, *ACS Energy Lett.*, 2019, **4**, 844–845.
2 A. Kojima, K. Teshima, Y. Shirai and T. Miyasaka, *J. Am. Chem. Soc.*, 2009, **131**, 6050–6051.
3 S. Lou, T. Xuan and J. Wang, *Opt. Mater.: X*, 2019, **1**, 100023.
4 P.-K. Kung, M.-H. Li, P.-Y. Lin, J.-Y. Jhang, M. Pantaler, D. C. Lupascu, G. Grancini and P. Chen, *Sol. RRL*, 2020, **4**, 1900306.
5 H. Yin, Y. Xian, Y. Zhang, W. Li and J. Fan, *Sol. RRL*, 2019, **3**, 1900148.
6 X. Han, J. Liang, J.-H. Yang, K. Soni, Q. Fang, W. Wang, J. Zhang, S. Jia, A. A. Martí, Y. Zhao and J. Lou, *Small*, 2019, **15**, 1901650.
7 M. Wang, P. Zeng, S. Bai, J. Gu, F. Li, Z. Yang and M. Liu, *Sol. RRL*, 2018, **2**, 1800217.
8 B. Wang, L. Yang, C. Dall'Agnese, A. K. Jena, S.-I. Sasaki, T. Miyasaka, H. Tamiaki and X.-F. Wang, *Sol. RRL*, 2020, **4**, 2000166.
9 G. Liu, C. Wu, Z. Zhang, Z. Chen, L. Xiao and B. Qu, *Sol. RRL*, 2020, **4**, 2000056.
10 C. J. Bartel, J. M. Clary, C. Sutton, D. Vigil-Fowler, B. R. Goldsmith, A. M. Holder and C. B. Musgrave, *J. Am. Chem. Soc.*, 2020, **142**, 5135–5145.
11 L. Mao, S. M. L. Teicher, C. C. Stoumpos, R. M. Kennard, R. A. DeCrescent, G. Wu, J. A. Schuller, M. L. Chabinyc, A. K. Cheetham and R. Seshadri, *J. Am. Chem. Soc.*, 2019, **141**, 19099–19109.
12 H. L. Wells, *Am. J. Sci.*, 1922, **3**, 315–326.
13 J. G. Bednorz and K. A. Müller, *Z. Phys*, 1986, **64**, 189–193.
14 N. Matsushita, H. Kitagawa and N. Kojima, *Acta Crystallogr., Sect. C: Cryst. Struct. Commun.*, 1997, **53**, 663–666.
15 N. Kojima, M. Hasegawa, H. Kitagawa, T. Kikegawa and O. Shimomura, *J. Am. Chem. Soc.*, 1994, **116**, 11368–11374.
16 N. Kojima, *Bull. Chem. Soc. Jpn.*, 2000, **73**, 1445–1460.
17 L. Debbichi, S. Lee, H. Cho, A. M. Rappe, K.-H. Hong, M. S. Jang and H. Kim, *Adv. Mater.*, 2018, **30**, 1707001.
18 K. Florian, *Z. Naturforsch. B*, 2011, **66**, 871–872.
19 H. Kitagawa, N. Kojima and T. Nakajima, *J. Chem. Soc., Dalton Trans.*, 1991, 3121–3125.
20 H. Kitagawa, N. Kojima and H. Sakai, *J. Chem. Soc., Dalton Trans.*, 1991, 3211–3215.
21 H. Fujiwara, M. Kato, M. Tamakoshi, T. Miyadera and M. Chikamatsu, *Phys. Status Solidi A*, 2018, **215**, 1700730.
22 A. D. Wright, R. L. Milot, G. E. Eperon, H. J. Snaith, M. B. Johnston and L. M. Herz, *Adv. Funct. Mater.*, 2017, **27**, 1700860.
23 S. D. Stranks and H. J. Snaith, *Nat. Nanotechnol.*, 2015, **10**, 391.
24 M. Roy, S. B. Vikram, A. Mitra, A. Alam and M. Aslam, *Chem. – Eur. J.*, 2019, **25**, 9892–9901.
25 T. K. Rose, *J. Chem. Soc., Dalton Trans.*, 1895, **67**, 881–904.
26 B. Ghosh, B. Febriansyah, P. C. Harikesh, T. M. Koh, S. Hadke, L. H. Wong, J. England, S. G. Mhaisalkar and N. Mathews, *Chem. Mater.*, 2020, **32**, 6318–6325.
27 C. Worley, A. Yangui, R. Roccanova, M.-H. Du and B. Saparov, *Chem. – Eur. J.*, 2019, **25**, 9875–9884.
28 H. Murasugi, S. Kumagai, H. Iguchi, M. Yamashita and S. Takaishi, *Chem. – Eur. J.*, 2019, **25**, 9885–9891.

